

FeZnSb₂: A possible NiAs-type hexagonal superconductor

Phinifolo Cambalame^{1,2}

¹ Centre for Physics of the University of Coimbra

² Department of Physics, Eduardo Mondlane University
phinifolo@fis.uc.pt

ABSTRACT

We present a first-principles investigation of electronic structure, lattice dynamics, and electron-phonon coupling of NiAs-type structure FeZnSb₂ and the isostructural parent compound FeSb within the framework of density functional theory. The calculation on partial disordered system FeZnSb₂ was performed in a fixed configuration. This hypothetical ordered structure is predicted to be superconducting.

General Terms

NiAs-type structure, partial disordered systems, superconductivity in Iron-based compounds

Keywords

NiAs-type structure, superconductivity, disordered partial systems

1. INTRODUCTION

The recent discovery of superconductivity in the NiAs-type structure high-entropy compound M_{1-x}Pt_xSb (M = equimolar Ru, Rh, Pd and Ir) [8] triggered our interest in the exploration of isostructural systems. Concurrently, the discovery of Fe-based pnictide and chalcogenide superconductors with high superconducting transition temperature (T_c) [10] has led to enormous excitement and opening of new perspective to develop a promising new platform to realize high- T_c superconductors. Among these, FeZnSb₂ stands out - an unexplored Fe-based system that has a NiAs-type structure with disordered atomic positions of Fe and Zn ($2a$ Wyckoff position) while Sb atoms occupy the $2c$ position according to [2] who first reported this system, derived from FeSb compound. To our knowledge, superconductivity has not been reported in an Fe-based compound with hexagonal structure, though the simple binary system FeSe, can crystallize in the superconducting phase β -FeSe (tetragonal) and δ -FeSe (hexagonal) non-superconducting phase [25, 16, 13]. The occurrence of superconductivity within disordered NiAs-type structures [8] or enhancement of T_c through disorder in other crystal systems [12] and the potential for ferroelectricity within distorted NiAs-type structures [24] render this material a confluence of features of great interest for both theoretical investigations and experimental studies. Disordered systems and partial ordered systems can also exhibit magnetic frustrated phases [17], spin-glass [23] due to complex exchange interactions between

the magnetic atoms introduced by the atomic disorder [20]. Partial ordered system generally have at least one ordered atomic position and remaining position randomly occupied. Fixed atomic configurations are relatively straightforward to handle and can yield data for comparison with experiments. Experimental parameters such as phonon vibrations and electronic structure can be calculated to infer the degree of disorder present in this system. Some systems with 50 % chemical scattering centers have already been observed to display superconductivity almost equal to pure elements [14].

In our current investigation, we present an *ab initio* prognosis regarding the superconductivity and stability of FeZnSb₂, under the assumption of fixed atomic positions for Zn and Fe. Our study entails the structural optimization of these compounds, juxtaposing the electronic structure and lattice dynamics of FeZnSb₂ with its parent compound, FeSb.

2. COMPUTATIONAL METHODS

The DFT calculations were carried out on QUANTUM-ESPRESSO version 7.2 [5, 4, 6] using SSSP PBE Precision v1.2.0 pseudopotentials [18], except when mentioned otherwise. The crystal visualization was carried on Xcrysden software [11]. The electronic band structure calculation were performed on relaxed structure, sampling the Brillouin zone (BZ) with $16 \times 16 \times 12$ k-points in the irreducible Brillouin zone (IBZ) with a 0.02 Ry smearing for BZ integration. The kinetic energy cutoff for wavefunctions was chosen to be 60 Ry and 420 Ry for charge density and potential for electronic structure and lattice dynamics calculations. As we are interested in superconductivity in the framework of DFT, other correlations effects beyond the DFT are not taken into account. Subsequently, to calculate the phonon dispersion curves and electron-phonon coupling we have employed density functional perturbation theory (DFPT), also within QUANTUM-ESPRESSO, using $20 \times 20 \times 16$ electronic k-point grids and $5 \times 5 \times 4$ phononic q-point grids.

3. RESULTS

3.1 Mechanical and Lattice Parameters

As mentioned earlier, FeZnSb₂ is a partially disordered system with NiAs-type crystal structure, while the Sb atoms occupy exclusively the As- crystal site in NiAs, the Ni ($2a$) site is now occupied by Zn and Fe. The translational asymmetric unit cell representation gives two equivalent atomic site, that were attribute randomly to

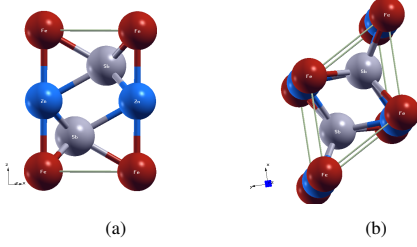


Fig. 1: FeZnSb₂. (a) View to xz-plane and (b) xy-plane view.

Zn and Fe atoms, resulting in the fixed or ordered configuration as depicted in Fig. 1, with the iron unit cell occupying the corner of the unit cell, and the zinc atoms in the intermediate edge position between the Fe atoms. The inverse occupation (Zn and Fe interchanged) gives the same Fermi surface and phonon dispersions and electron-phonon coupling strength, as could be expected. In FeSb, we have a similar picture, with the obvious difference being that Zn is now replaced by Fe atoms.

Table 1.: Equilibrium crystal lattice parameters, a and b , Bulk modulus B and total energy E_{min} .

	a	b	B (GPa)	E_{min} (Ry)
FeSb	3.99	4.97	140.4	-1028.4026
Exp. [22]	4.1	5.14	—	—
FeZnSb ₂	4.19	5.17	82.4	-1160.70637
Exp. [2]	4.38	5.73	—	—

The optimization of the crystal structure from the experimental lattice parameters [22, 2] provides good agreement between experimental and relaxed structure for FeSb but not in the FeZnSb₂ case. There's 10% disagreement of the c lattice parameter, while for both FeSb lattice parameters this underestimation falls around 3% (see Table 1). To understand this uncommon underestimation of cell volume (and the c lattice constant, in particular) we performed a series of calculations with FeZnSb₂ supercells of $2 \times 2 \times 2$ dimensions [21], where the theoretical sites of Zn and Fe were gradually interchanged, the results are plotted at Fig. 2. Our calculations suggest that the increment of disorder in system, will shrink the unit cell volume. This result rules out disorder in the Zn and Fe positions as the primary cause for the abnormal underestimation of the lattice constant, thereby suggesting the potential involvement of other interactions, such as magnetism, in this discrepancy. We advance that the diffusion of Fe (or Zn) to the double tetrahedral interstitial positions within the primitive unit cell [19] constitutes the primary factor. This phenomenon has been previously documented in FeSb, NiSb, and related structures [7]. Afterwards, we have performed magnetic calculations with different magnetic states and have come to the conclusion that the ground state of FeSb is ferromagnetic (FM), while for FeZnSb₂, the FM state and collinear antiferromagnetic (AFM) state are separated by a mere 2 mRy (calculation on $2 \times 1 \times 1$ supercell). While the FM state predominates as the lowest-energy configuration, this small difference suggests a more complex ground state and more detailed calculations is needed to elucidate further.

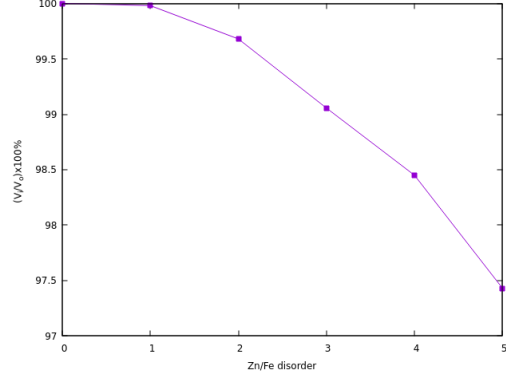


Fig. 2: Variation of ordered FeZnSb₂ with the Zn/Fe iter-site substitution

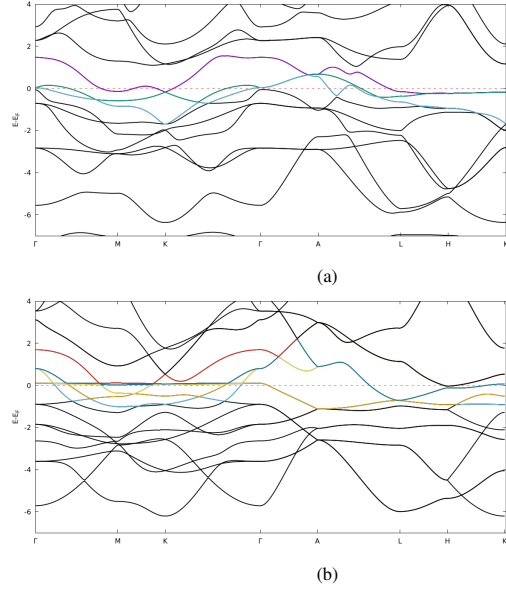


Fig. 3: Electronic structure of (a) FeZnSb₂ and (b) FeSb.

3.2 Electronic Structure

The calculated electronic band structure are shown in Fig. 3. There are relatively more bands crossing the Fermi level in FeSb (Fig. 3b) than in FeZnSb₂ (Fig. 3a). There are multiple flat bands above the Fermi level along the Γ -M-K- Γ in FeSb, and in FeZnSb₂ two degenerate flat bands along the L-H-K high-symmetry path are observed. The projected band structure calculations for FeZnSb₂ suggest a splitting into two sets of doubly degenerate states: one of the d_{xz} and d_{yz} character and another of the $d_{x^2-y^2}$ and d_{xy} character, along with a non-degenerate state derived from the d_{z^2} orbital. Unlike the FeZnSb₂ degeneracy picture, where we have a complete degeneracy along the displayed high-symmetry path (Fig. 3a), the set of d_{xz} and d_{yz} in FeSb have their degeneracy lifted along the A-L-H path, the set of $d_{x^2-y^2}$ and d_{xy} are partially degenerate only close to the Fermi level and significantly along M-K- Γ -A and lifted elsewhere. In FeZnSb₂, there's a significant hybridization between Sb (p_x and p_y) with Fe ($d_{x^2-y^2}$). Hybridization is marginally in FeSb.

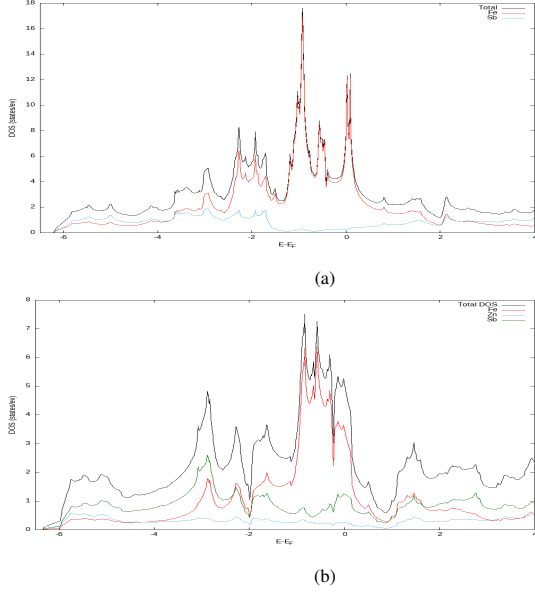


Fig. 4: Total and partial density of state (DOS) (a) for FeSb and (b) FeZnSb₂.

The density of states at the Fermi level of these two materials exhibits a metallic behaviour (see Fig. 4). The contribution of Sb to the density of states is higher in FeZnSb₂ than in FeSb. This can be explained by the stronger covalent binding between Sb and Fe in the former compound. The contribution of Zn to the total DOS of FeZnSb is marginal. In both FeSb and FeZnSb₂ the highest DOS is observed along the L-H-K near the Fermi Level.

3.2.1 Fermi surfaces. At the Γ point, we observe the primary topological difference in the Fermi surface (FS) see Fig. 5 and 6. In FeSb, we identify two anisotropic and co-centered 2-D hole pocket, whereas in FeZnSb₂ a cylinder-like structure encloses a complex dumbbell-like formation. In these two systems, we observe along the boundaries a typical metallic open FS extending over almost the entire BZ.

3.3 Phonons and electron-phonon coupling

The calculated phonon dispersion curves are shown in Fig. 7. The absence of any imaginary or negative vibrational modes suggests that both FeZnSb₂ and FeSb are dynamically stable systems within a hexagonal structure of NiAs-type. The origin of phonon branches is similar; the highest frequency branches result from the contribution of Fe and Zn in FeZnSb₂ and Fe in FeSb. The three (two) atomic species are involved in the acoustic vibration modes of FeZnSb₂ (FeSb). This pattern of vibration explains the depression in the phonon DOS when transiting to high frequencies. Raman and infrared (IR) were calculated at Γ . The calculation on the FeZnSb₂ (FeSb) relaxed structure assigns the crystallographic symmetry to D_{3d} (C_{2v}), which decomposes into the vibrational modes in (Γ) to the following irreducible representations:

$$\Gamma = 3A_{2u} + 3E_u + E_g + A_{1g} \quad (1)$$

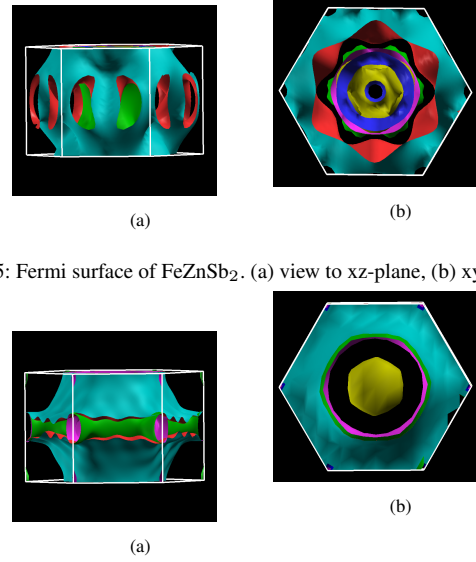


Fig. 5: Fermi surface of FeZnSb₂. (a) view to xz-plane, (b) xy-plane view.

Fig. 6: Fermi surface FeSb. (a) view to xz-plane, (b) xy-plane view.

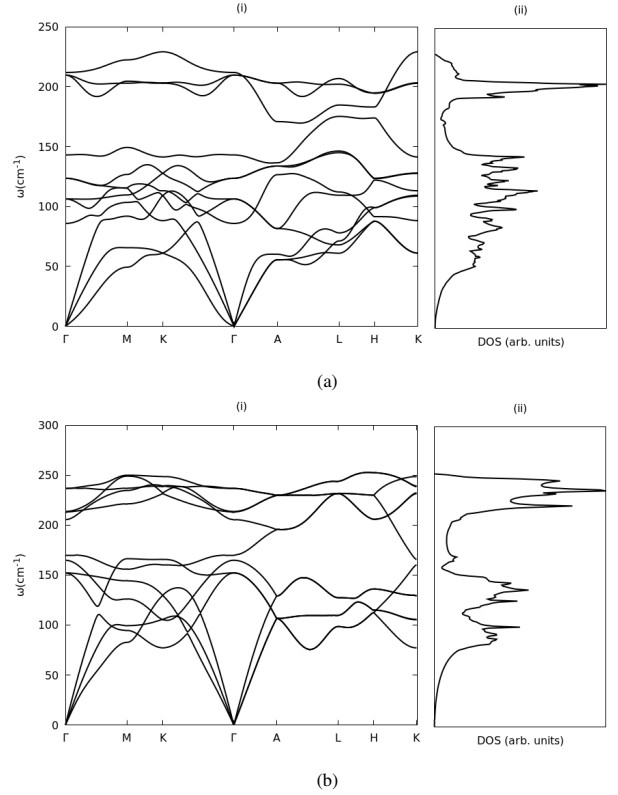


Fig. 7: Phonon dispersion curves along high symmetry curves and the density of states (DOS) (a) for FeZnSb₂ and (b) FeSb .

Table 3. : The calculated DOS at E_F , $N(0)$, the average electron-phonon coupling constant λ , the logarithmically averaged ω_{log} phonon frequencies and T_c calculated from modified McMillan formula eqn. 2

	$N(0)$	λ	$\omega_{log}[K]$	$T_c[K] (\mu = 0.1)$
FeSb	39.471550	0.33	191.886	0.217
FeZnSb ₂	21.530679	0.59	139.067	3

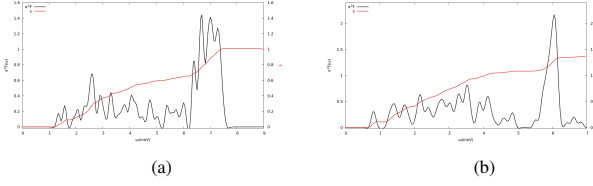


Fig. 8: Electron-phonon spectral function $\alpha^2 F(\omega)$ and cumulative electron-phonon coupling strength λ for (a) FeSb and (b) FeZnSb₂

Table 2. : The calculated frequencies of the Raman (R) and infrared (I) active modes of FeSb and FeZnSb₂. The modes are classified by the irreducible representations (irrep) according to which they transform.

FeSb		FeZnSb ₂		
$\omega \text{ cm}^{-1}$	(irrep)		$\omega \text{ cm}^{-1}$	(irrep)
8.1	(B ₁)	I+R	11.3	(A _{2u}) I
152.1	(A ₁ , B ₂)	I+R	17.7	(E _u) I
164.8	(A ₂)	R	88.2	(A _{2u}) I
170.5	(B ₁)	I+R	108.1	(E _u) I
205.9	(B ₂)	I+R	125.3	(E _g) R
213.3	(A ₂)	R	143.1	(A _{1g}) R
213.7	(B ₁)	I+R	209.3	(E _u) I
236.8	(A ₁)	I+R	212.7	(A _{2u}) I

The calculated Raman and infrared active modes can be validated through experimentation, enabling inference about the disorder of the system and its crystallographic symmetry, particularly in the case of FeZnSb₂. The E_g Raman mode exhibits degeneracy. Both Raman modes are attributed exclusively to Sb vibrations in FeZnSb₂, whereas in FeSb, one Raman mode (164.8 cm^{-1}) originates from Sb and 213.13 cm^{-1} from Fe. The presence of flat bands in this material may suggest low thermal conductivity and potential thermoelectric capacity [3].

3.3.1 Electron-phonon coupling and superconductivity. The frequency dependence of the Eliashberg spectral function $\alpha^2 F(\omega)$ and the average λ value for FeSb and FeZnSb₂ are presented in Table 3 and Fig. 8. We have also calculated the relevant parameters for the description of the superconducting properties within the Eliashberg formalism, namely the logarithmically averaged phonon frequency ω_{log} and the superconducting transition temperature T_c , calculated by the McMillan [15] formula modified by Allen-Dynes [1] Eq. 2, presented in the table 3.

$$T_c = \frac{\omega_{log}}{1.2} \exp\left(-\frac{1.04(1+\lambda)}{\lambda - \mu^*(1+0.62\lambda)}\right) \quad (2)$$

To validate the accuracy of our findings, we conducted a fresh computation employing the projector augmented-wave (PAW) pseudopotentials [9] version 2.0.1, yielding closely aligned results.

Specifically, we observed an average T_c of 3.7 K and an electron-phonon coupling strength of 0.66.

3.4 Discussion and conclusions

In this study, we demonstrate the stability of synthesized compounds FeSb and FeZnSb₂ with the NiAs structure. The simulated disorder in FeZnSb₂ reveals that the lattice parameter will shrink with disorder, and the substitution of Fe by Zn increases the relevance of Sb in the DOS next to the Fermi level. If the phonon mediated pairing mechanism for superconductivity is assumed for these systems, superconducting transition temperature is expected to be significant in the unexplored system FeZnSb₂. While disorder within the system may negatively impact superconductivity, the potential occurrence of superconductivity in this Fe-based compound offers a novel platform for material manipulation and comparison with unconventional superconductors, particularly Fe-based layered compounds. The findings of this theoretical study serve as strong motivation for the synthesis and experimental exploration of this compound, as well as for employing more sophisticated methodologies in theoretical calculations. This includes the introduction of supercells and disorder to better align with the realistic characteristics of the FeZnSb₂ system.

ACKNOWLEDGMENTS

This work was produced with the support of CFISUC computing resources, cluster Adamastor.

4. REFERENCES

- [1] P. B. Allen and R. C. Dynes. Transition temperature of strong-coupled superconductors reanalyzed. *Phys. Rev. B*, 12:905–922, Aug 1975.
- [2] I.V Chumak, V.V Pavlyuk, G.S Dmytriv, and J Stepień-Damm. Phase equilibria and crystal structure of compounds in the Fe–Zn–Sb system at 570 K. *Journal of Alloys and Compounds*, 307(1):223–225, 2000.
- [3] DD Fan, HJ Liu, L Cheng, J Zhang, PH Jiang, J Wei, JH Liang, and J Shi. Understanding the electronic and phonon transport properties of a thermoelectric material BiCuSeO: a first-principles study. *Physical Chemistry Chemical Physics*, 19(20):12913–12920, 2017.
- [4] P Giannozzi, O Andreussi, T Brumme, O Bunau, M Buongiorno Nardelli, M Calandra, R Car, C Cavazzoni, D Ceresoli, M Cococcioni, N Colonna, I Carnimeo, A Dal Corso, S de Gironcoli, P Delugas, R A DiStasio Jr, A Ferretti, A Floris, G Fratesi, G Fugallo, R Gebauer, U Gerstmann, F Giustino, T Gorni, J Jia, M Kawamura, H-Y Ko, A Kokalj, E Küçükbenli, M Lazzeri, M Marsili, N Marzari, F Mauri, N L Nguyen, H-V Nguyen, A Otero de-la Roza, L Paulatto, S Poncé, D Rocca, R Sabatini, B Santra, M Schlipf, A P Seitsonen, A Smogunov, I Timrov, T Thonhauser, P Umari, N Vast, X Wu, and S Baroni. Advanced capabilities for materials modelling with QUANTUM ESPRESSO. *Journal of Physics: Condensed Matter*, 29(46):465901, 2017.
- [5] Paolo Giannozzi, Stefano Baroni, Nicola Bonini, Matteo Calandra, Roberto Car, Carlo Cavazzoni, Davide Ceresoli, Guido L Chiarotti, Matteo Cococcioni, Ismaila Dabo, Andrea Dal Corso, Stefano de Gironcoli, Stefano Fabris, Guido Fratesi, Ralph Gebauer, Uwe Gerstmann, Christos Gougousis, Anton Kokalj, Michele Lazzeri, Layla Martin-Samos,

- Nicola Marzari, Francesco Mauri, Riccardo Mazzarello, Stefano Paolini, Alfredo Pasquarello, Lorenzo Paulatto, Carlo Sbraccia, Sandro Scandolo, Gabriele Scлаuzero, Ari P Seitsonen, Alexander Smogunov, Paolo Umari, and Renata M Wentzcovitch. QUANTUM ESPRESSO: a modular and open-source software project for quantum simulations of materials. *Journal of Physics: Condensed Matter*, 21(39):395502 (19pp), 2009.
- [6] Paolo Giannozzi, Oscar Barone, Pietro Bonfà, Davide Brunato, Roberto Car, Ivan Carnimeo, Carlo Cavazzoni, Stefano de Gironcoli, Pietro Delugas, Fabrizio Ferrari Ruffino, Andrea Ferretti, Nicola Marzari, Iurii Timrov, Andrea Urru, and Stefano Baroni. Quantum ESPRESSO toward the exascale. *The Journal of Chemical Physics*, 152(15):154105, 2020.
- [7] R. Hanel, W. Miekeley, and H. Wever. Diffusion studies on the B8 phase of the Ni/Sb system. *physica status solidi (a)*, 97(1):181–190, 1986.
- [8] Daigorou Hirai, Naoto Uematsu, Koh Saitoh, Naoyuki Katayama, and Koshi Takenaka. Superconductivity in High-Entropy Antimonide $M_{1-x}Pt_xSb$ ($M = \text{Equimolar Ru, Rh, Pd, and Ir}$). *Inorganic Chemistry*, 62(35):14207–14215, 2023. PMID: 37602725.
- [9] François Jollet, Marc Torrent, and Natalie Holzwarth. Generation of Projector Augmented-Wave atomic data: A 71 element validated table in the XML format. *Comput. Phys. Commun.*, 185:1246, 2014.
- [10] Yoichi Kamihara, Takumi Watanabe, Masahiro Hirano, and Hideo Hosono. Iron-Based Layered Superconductor $La[O_{1-x}F_x]FeAs$ ($x = 0.05-0.12$) with $T_c = 26$ K. *Journal of the American Chemical Society*, 130(11):3296–3297, 2008. PMID: 18293989.
- [11] Anton Kokalj. XCrySDen—a new program for displaying crystalline structures and electron densities. *Journal of Molecular Graphics and Modelling*, 17(3):176–179, 1999.
- [12] M. Lehmann, G. Saemann-Ischenko, H. Adrian, and C. Nölscher. Disordered A15 compounds from the Matthias-Valley: Mo_3Ge and Mo_3Si . *Physica B+C*, 107(1):473–474, 1981.
- [13] Hechang Lei, Rongwei Hu, and C. Petrovic. Critical fields, thermally activated transport, and critical current density of β -FeSe single crystals. *Phys. Rev. B*, 84:014520, Jul 2011.
- [14] B.T. Matthias, E.A. Wood, E. Corenzwit, and V.B. Bala. Superconductivity and electron concentration. *Journal of Physics and Chemistry of Solids*, 1(3):188–190, 1956.
- [15] W. L. McMillan. Transition Temperature of Strong-Coupled Superconductors. *Phys. Rev.*, 167:331–344, Mar 1968.
- [16] D. Mendoza, J.L. Benítez, F. Morales, and R. Escudero. Magnetic anomaly in superconducting FeSe. *Solid State Communications*, 150(25):1124–1127, 2010.
- [17] Santanu Pakhira, Chandan Mazumdar, R Ranganathan, and Maxim Avdeev. Magnetic frustration induced large magnetocaloric effect in the absence of long range magnetic order. *Scientific Reports*, 7(1):7367, 2017.
- [18] Gianluca Prandini, Antimo Marrazzo, Ivano E Castelli, Nicolas Mounet, and Nicola Marzari. Precision and efficiency in solid-state pseudopotential calculations. *npj Computational Materials*, 4(1):72, 2018. <http://materialscloud.org/sssp>.
- [19] M. Sladecek, M. Miglierini, B. Sepiol, H. Ipser, H. Schickentanz, and G. Vogl. Diffusion Mechanism in the Hexagonal B8 Structure of FeSb. In *Diffusion in Materials DIMAT2000*, volume 194 of *Defect and Diffusion Forum*, pages 369–374. Trans Tech Publications Ltd, 4 2001.
- [20] Maria Szlowska, Daniel Gnida, and Dariusz Kaczorowski. Magnetic and electrical transport behavior in the crystallographically disordered compound U_2CoSi_3 . *Phys. Rev. B*, 84:134410, Oct 2011.
- [21] Atsushi Togo, Laurent Chaput, Terumasa Tadano, and Isao Tanaka. Implementation strategies in phonopy and phono3py. *J. Phys. Condens. Matter*, 35(35):353001, 2023.
- [22] EA Vasilev and VA Virchenko. Solid solutions in the $(Fe_{1.22}Sb)_{1-x}(Fe_{1.68}Sn)_x$ system. *physica status solidi (a)*, 70(2):K141–K143, 1982.
- [23] Yurong You, Guizhou Xu, Jiaxuan Tang, Chao Li, Jun Liu, Yuanyuan Gong, and Feng Xu. Spin-glass mediated large exchange bias and coercivity in hexagonal $Mn_{1+x}Cu_{1-x}Ga$ ($x = 0.3-0.5$) alloys. *Journal of Physics D: Applied Physics*, 53(26):265001, apr 2020.
- [24] Hu Zhang, Bei Deng, Wei-Chao Wang, and Xing-Qiang Shi. Class of diatomic ferroelectrics with multifunctional properties: IV-VI compounds in the distorted NiAs-type structure. *Phys. Rev. B*, 96:245136, Dec 2017.
- [25] S B Zhang, X D Zhu, H C Lei, G Li, B S Wang, L J Li, X B Zhu, Z R Yang, W H Song, J M Dai, and Y P Sun. Superconductivity of $FeSe_{0.89}$ crystal with hexagonal and tetragonal structures. *Superconductor Science and Technology*, 22(7):075016, jun 2009.